MetaSense: Integrating Sensing Capabilities into Mechanical Metamaterial
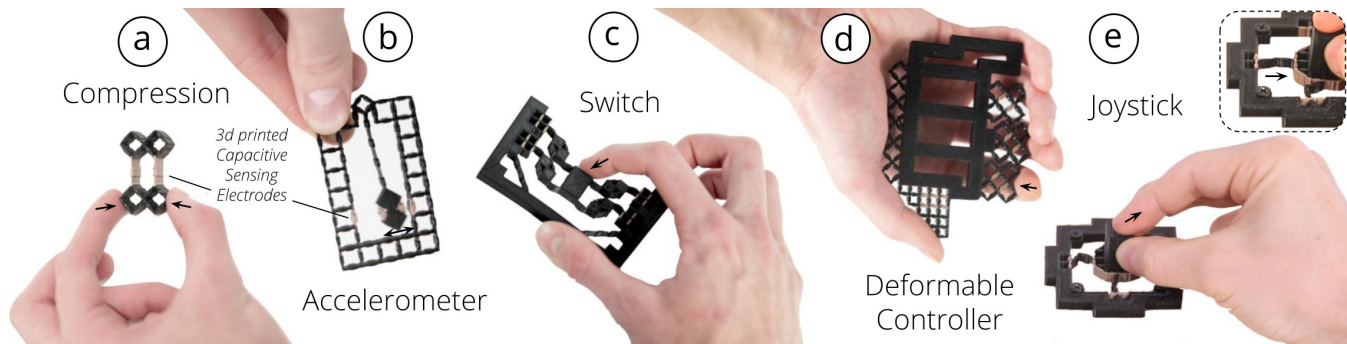
Jun Gong*
Apple/MIT CSAIL
Seattle, WA, USA
jungong@mit.edu

Olivia Seow*
MIT CSAIL
Cambridge, MA, USA
olivias@mit.edu

Cedric Honnet*
MIT Media Lab
Cambridge, MA, USA
honnet@mit.edu

Jack Forman
MIT Media Lab
Cambridge, MA, USA
jackform@media.mit.edu

Stefanie Mueller
MIT CSAIL
Cambridge, MA, USA
stefanie.mueller@mit.edu

Figure 1: MetaSense integrates sensing into 3D printable metamaterial structures by fabricating specific cell walls from conductive filament, thereby creating electrodes that can be used for capacitive sensing: (a) an input device that senses compression, (b) an accelerometer, (c) a discrete state switch, (d) a controller that senses shear, and (e) a joystick that senses magnitude and direction of applied force.

ABSTRACT

In this paper, we present a method to integrate sensing capabilities into 3D printable metamaterial structures comprised of cells, which enables the creation of monolithic input devices for HCI. We accomplish this by converting select opposing cell walls within the metamaterial device into electrodes, thereby creating capacitive sensors. When a user interacts with the object and applies a force, the distance and overlapping area between opposing cell walls change, resulting in a measurable capacitance variation.

To help designers create interactive metamaterial devices, we contribute a design and fabrication pipeline based on multi-material 3D printing. Our 3D editor automatically places conductive cells in locations that are most affected by deformation during interaction and thus are most suitable as sensors. On export, our editor creates two files, one for conductive and one for non-conductive cell walls, which designers can fabricate on a multi-material 3D printer. Our applications show that designers can create metamaterial devices that sense various interactions, including sensing acceleration, binary state, shear, and magnitude and direction of applied force.

CCS CONCEPTS

• **Human-centered computing** → **Human computer interaction (HCI)**.

KEYWORDS

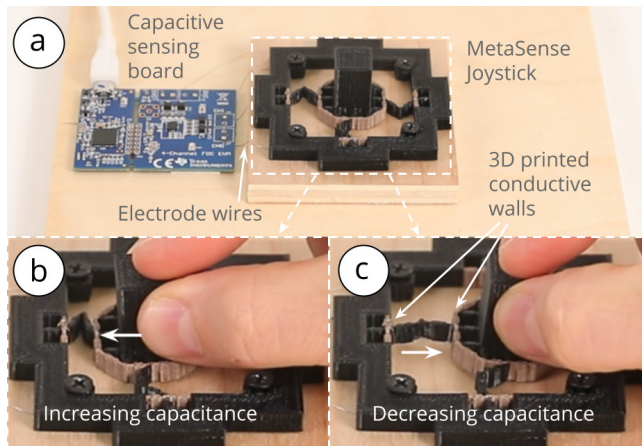Personal Fabrication, Metamaterials, Capacitive Sensing, Multi-material Printing.

*authors contributed equally

1 INTRODUCTION

While early work in personal fabrication focused on designing the outside of objects, recently researchers proposed to also consider

Figure 2: The conductive cell walls of MetaSense objects act as capacitance sensors to detect user interaction. Here, a Metasense joystick is shown in (a) original state and (b,c) deformed states during user interaction with capacitance changes of conductive shear cells detected accordingly.

the internal structure of objects as an important design element [3]. By dividing the inside of objects into grids of repetitive cells and modifying the parameters of the cells, researchers were able to achieve various mechanical properties. These so called mechanical metamaterials [24] can make objects harder or softer [22] and more or less flexible [9] through their specific internal geometries without changing the outer geometry or printing material. To push this idea further, Ion et. al. proposed metamaterial mechanisms [13], which are cell structures that transmit input forces in one location to output forces in another when cells are being deformed.

To augment such mechanical metamaterial structures with sensing capabilities, researchers investigated how to integrate different types of sensing elements. For instance, Helou et al. [10] and Nick et al. [19] showed how to embed discrete digital switches and logic gates into mechanical metamaterials. However, while these works are able to sense discrete states when the metamaterial structure is being deformed, they are not able to continuously sense deformation. In addition, the sensing elements are created by either manually filling liquid metal channels inside the metamaterial [19] or by applying conductive ink to the passive metamaterial structure [10]. Furthermore, placing the sensing elements inside the metamaterial structure requires expertise and no support tool was provided by these prior works to help users with quickly prototyping metamaterial structures with various sensing capabilities.

In this paper, we explore how to go beyond sensing discrete states by developing an approach to add continuous deformation sensing to mechanical metamaterials. Inspired by work on conductive shear cells as sensors [7, 26], we propose to integrate these cells into mechanical metamaterial devices. Each conductive shear cell contains two opposing conductive walls. When a user is manipulating the metamaterial device, the distance and overlap area between the two opposing conductive walls of a cell change accordingly, resulting in a capacitance variance that can be measured. This is depicted in Figure 1e and Figure 2.

To help designers create mechanical metamaterial devices with continuous deformation sensing, we built a 3D editor that computes the optimal locations for placing conductive shear cells within the structure. We accomplish this by running a mechanical simulation which identifies the cell walls with the greatest deformation and thus the greatest capacitance variation, which are ideal candidate locations for sensing cells. On export, the editor creates two .stl files for multi-material 3D printing with conductive and non-conductive filament, eliminating the need for manual assembly. After 3D printing, users only have to connect the conductive cell walls to our sensing hardware and the interactive object is ready be to be used. To evaluate the effectiveness of our approach, we tested conductive shear cells of varying sizes and found that even small cell sizes (5mm x 5mm) support robust capacitive sensing.

In summary, our primary contributions are: (1) the development of metamaterial devices with continuous deformation sensing enabled by measuring capacitance variation caused by the deformation of conductive shear cells, (2) a design and fabrication pipeline based on multi-material 3D printing that supports designers in placing conductive shear cells in optimal sensing locations based on a simulation of mechanical deformation, (3) a study to validate the feasibility of our sensing approach with different cell parameters (e.g., thickness, width); and (4) a series of applications to showcase the sensing capabilities and interactions enabled by our technique.

2 RELATED WORK

Our work builds on research in adding sensing to printed objects, designing the interior of objects, and multi-material design tools.

2.1 Adding Sensing to 3D Printed Objects

While most personal fabrication research focused on adding sensing to objects manually by attaching conductive copper tape (Midas [28], SurfCuit [37]), filling internal pipes with conductive paint or silicone (A Series of Tubes [27], CurveBoards [43]), spraying conductive inks onto objects (Sprayable User Interfaces [41]), or assembling parts printed separately by a metal 3D printer (SteelSense [38]), recent advances in multi-material FDM 3D printing with conductive filament enabled researchers to print interactive objects with sensing elements in one go using low-cost hardware.

The first sensors that were created using conductive filament were different types of capacitive touch sensing elements. For instance, PrintPut [6] Capricate [29], Electrick [42], and ./Trilaterate [31] showed how to create touch buttons, sliders, dials, and multi-touch pads by printing with conductive and non-conductive material. Conductive filament has also been used by researchers to develop 3D printed objects that support two factor authentification (3D-Auth [17]) and connect with each other wirelessly (Printed Wifi [15]). More recently, conductive filament has been used to detect object deformation. While prior research created deformation sensors by casting silicone [8, 35] or attaching copper tape to shear structures (Foldio [21]), researchers showed that deformation sensing can also be achieved by printing parts of the object with conductive filament (Flexibles [30]).

One way to sense deformation is to integrate electrodes made from conductive material into a shearing mechanisms as demonstrated by the conductive shear cell design from Sarwar et al. [26]

and Chase et al. [7]. Foldio [21] shows how to integrate these conductive shear cells into 2D folded paper structures to sense shearing directions (e.g., right or left). However, their work focuses solely on 2D structures and cannot sense continuous distance change between electrodes. In our work, we integrate the conductive shear cell into 3D printable metamaterial structures to enable continuous sensing of interaction.

2.2 Interior Design of Printed Objects

Research in mechanical engineering and computer graphics has shown how the design of an object's internal structure (e.g., object infill) can help optimize structural parameters, such as improving the strength-to-weight ratio of an object [16] or shifting its center of mass [25]. More recently, researchers proposed the concept of mechanical metamaterials, which consist of repeating cell structures that depending on the specific cell design can modulate various mechanical properties without changing the outer object geometry (i.e. shape) [24]. Researchers have shown that interior cell design allows to modulate a variety of mechanical properties such as stiffness [23], elasticity [9, 32], and the damping coefficient [33]. Ion et. al. [13] extended the design space by also enabling the transmission of forces through the cell structure, thereby making them act like mechanisms. Being able to transmit forces also allowed Ion et al. to create simple logic functions [14]. In the last few years, researchers also started to add sensing capabilities to mechanical metamaterials in the form of discrete digital switches and logic gates [10, 19]. In our work, we extend the sensing capabilities by introducing a method to add continuous deformation sensing to metamaterials, which enables more comprehensive interaction sensing.

2.3 Multi-material Design Tools

Modeling multi-material 3D printed objects can be difficult since users have to translate the desired high-level functionality into low-level geometry, where each voxel of the printed object can potentially be made from a different material. To facilitate the design process, 3D modeling tools such as Netfabb [2] and Materialise 3-Matic [18] allow users to specify materials for different functional parts and then generate low-level geometry, such as lattices that create the specified functionality. OpenFab [40] allows users to assign shader-like fablets to 3D models, the shader is then translated into individual geometries and material assignments for 3D printing upon export. More recently, a multi-material fabrication design tool targeted at non-technical users, Foundry [39], was built to provide an interactive and visual process for designing spatially varying material properties. In our work, we facilitate the design of mechanical metamaterials with integrated deformation sensing by including different types of conductive shear cells as template shapes in our editor. On export, our editor automatically generates two mesh files for multi-material 3D printing, i.e. one for the conductive and one for the non-conductive part of the metamaterial structure.

3 SENSING TECHNIQUE

MetaSense objects are metamaterial devices with integrated deformation sensing. In this section, we discuss the sensing principle and resonance-based capacitive sensing technique used to create our interactive metamaterial devices.

3.1 Sensing Principle: Capacitance Change Between Conductive Cell Walls

As mentioned in the introduction, our conductive shear cells contain two conductive opposing walls. Each conductive wall serves as an electrode. When a user interacts with the object and applies a force, the geometry and consequently the conductive shear cells deform. The distance and overlapping area between two opposing conductive walls change accordingly, resulting in a capacitance change that can be measured via capacitive sensing.

3.2 Resonance-Based Capacitive Sensing

To sense this capacitance change, we use a resonance-based approach rather than a traditional time-based capacitance method. There are two main reasons for this.

High Measurement Resolution: Unlike conventional capacitive sensing for touch input, our application requires measuring small capacitance changes. This is caused by three factors. First, the conductive cell walls (i.e., the electrodes) are smaller than the electrodes traditionally used for touch sensing. Second, the electrodes are 3D printed with conductive filament, which has a high resistance, and thus the printed electrodes have a lower conductivity compared to metal electrodes of the same size. Third, the contact resistance between the wires and the printed electrodes results in a higher resistance reading than is theoretically possible. These factors cause capacitance changes to be small when the cells are deformed. A resonance-based measurement approach has a higher precision than time-based capacitance and allows us to compensate for the diminished conductivity. The resonance-based system allows us to detect capacitances across a 1pF to 250nF range [11]. In our experiments, capacitances ranged from 1.0029pF to 1.0857pF.

Better Signal-to-Noise Ratio: A resonance-based approach is less susceptible to electromagnetic interference (EMI) and thus has a better signal-noise-ratio (SNR). This further combats the issue of diminished electrode quality due to the aforementioned reasons.

## 3.3 Measuring Capacitance to Determine Shear

The capacitance C (in Farads) between two electrodes (i.e., two opposing conductive walls) is given by:

$$C = \epsilon_0 \frac{A}{d} = \epsilon_0 \frac{lw}{d} \tag{1}$$

where A is the area of overlap of the two electrodes (in m²), ϵ_0 is the electric constant of free space between the electrodes, and d is the distance between the electrodes (in m) as shown in Figure 3a. l and w are the length and width of the electrodes, i.e. the conductive walls (in m). In our case, the conductive walls are square electrode walls and thus l and w are equal.

When a conductive cell is shearing, the amount of overlap A and the distance d between the two conductive cell walls changes to A' and d' (Figure 3b), which leads to a different capacitance C.

Computing Capacitance (C): We compute the capacitance C between the two opposing conductive cell walls using a resonance-based approach as discussed in Section 3.2. We use an LC resonant circuit [12], which consists of an inductor and a capacitor (i.e., the two conductive walls). The capacitance C between two conductive walls of a resonance-based circuit is given by:
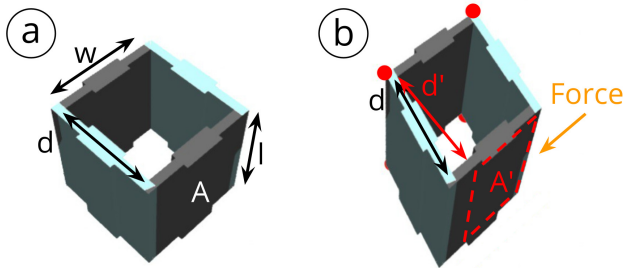
Figure 3: Measuring capacitance changes: (a) original state, (b) deformed state. *Perpendicular* distance d and *overlapping* area A in (a) changes after deformation to d' and A' respectively in (b).

$$C = \frac{1}{4\pi^2 f^2 L} \quad (2)$$

where L is the known inductance of the inductor (18mH) and f is the resonant frequency of the circuit. By measuring the resonant frequency f of the circuit, we can calculate the capacitance C between the two conductive walls in formula (2).

3.4 Sensing Hardware

To measure the resonant frequency f, we built a circuit consisting of a resonant-based capacitive sensing chip (FDC2214, Texas Instruments) and also used the evaluation board (FDC2214EVM) to collect the resonant frequency measurements (Figure 2a).

Sensing Resolution: We chose the capacitive sensing chip (FDC2214) for its high resolution (up to 28 bits) and intrinsic noise robustness to compensate for the low conductivity of the printed electrodes. After calibration, we needed up to 21bits out of the available 28bits, which exceeds the 10 bits offered by the common alternatives, i.e. the MPR121 chip or the Arduino *CapacitiveSensor* library. For applications that do not require a high sensing resolution, these advantages may not be imperative, and the alternative chips can be used as well.

Sampling Rate: The evaluation board can achieve measurements with a sampling rate of up to 13,300Hz. For our applications, a sampling rate of 100Hz (i.e., 100 samples per second) was sufficient, but higher sampling rates may be useful for higher frequency applications.

Number of Cell Walls Supported: The evaluation board can take resonant frequency measurements on up to four input channels, which allows us to measure four conductive cells at a time. By using a 4:1 multiplexer (FSUSB74, ON Semiconductor), we were able to increase the number of conductive cells that can be measured with the board to 16. Adding additional multiplexers can further increase the number of cells that can be measured simultaneously.

3.5 Signal Processing

After receiving the resonant frequency measurements, we used exponential smoothing (a special case of the IIR low-pass filter) to remove noise from the input data. We then converted the resonant frequencies to capacitances using formula (2). For calibration, we

compute the working range by memorizing the minimum and maximum measured values at each sample. For the user interactions, we only send a measurement percentage according to the working range.

3.6 Extension of Sensing Principle to Advanced Cell Types

The sensing principle described above also applies to cell types that are different from the standard cell shown in Figure 3. The non-conductive walls need not be parallel, and can take on different layouts. Figure 4 shows example configurations of advanced conductive shear cells that use the same sensing principle and are supported by the same measurement hardware as the conductive shear cell described in the previous sections. Depending on the situation, we might need special mechanical properties such as strength or flexibility, and these advanced cells allow better capacitance ranges, hence better signal-to-noise ratio.
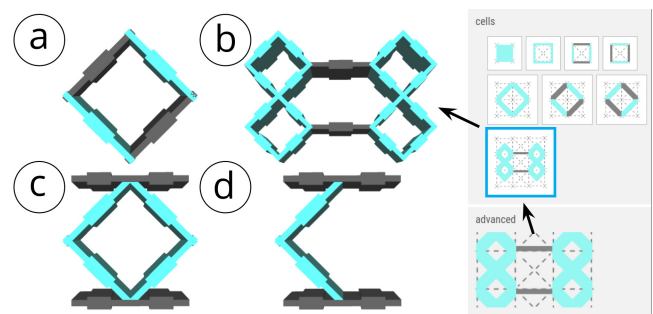
Figure 4: Examples of different types of conductive shear cells, all supported by the same sensing principle and sensing hardware: (a) is standard, (b) is used for our characterization, and (c,d) are used in the joystick.

4 FABRICATING OBJECTS WITH CONDUCTIVE SHEAR CELLS

To accomplish the best print quality for MetaSense objects, we experimented with different 3D printers, filaments, and print settings, and tested different methods to connect the printed cells to the sensing board.

3D Printer & Filament: We tested three different 3D printers (Ultimaker3, PRUSA i3 MK3 with multi-material add-on, and FlashForge New Creator Pro 2), two conductive filaments (ProtoPasta Composite Conductive PLA, Multi3D Electrifi) and two non-conductive filaments (NinjaFlex TPU, SainSmart Flexible TPU). Each 3D printer and filament combination required adjustments of the default settings to successfully print robust yet flexible multi-material objects containing conductive shear cells. The 3D printer and filament combination that produced the best result was the FlashForge New Creator Pro 2 (0.4mm nozzle) with the conductive filament Multi3D Electrifi (1.75mm, $0.006\Omega cm$ in copper) and the non-conductive flexible filament SainSmart (1.75mm in black or white). We used this 3D printer and filament combination to print the example objects in this paper.

Printing Settings: We determined that the optimal extrusion temperature for the conductive filament is 130°C and for the non-conductive filament 230°C. A print speed of 10mm/s produced sufficiently conductive cells, but slower print speeds led to higher conductivity at the expense of additional print time. We kept the build plate temperature relatively cool at 40°C since the lower melting point of the conductive material sometimes caused prints to detach during the build process. Lining the build plate with an even layer of masking tape followed by a coat of Elmer's All Purpose School Glue Stick helped to adhere the object to the build plate while it was being printed. We used a prime tower to prevent print residuals that occur when the 3D printer switches between the conductive and non-conductive filaments.

Connection to Sensing Board: After 3D printing, we connected the conductive cell walls to the sensing board using a bare nickel chromium wire (34-gauge). We first warmed the end of the wire, allowing it to more easily pierce through the conductive cell wall (as it slightly melts the filament), and then looped it around the cell wall once. We then soldered the other side of the wire to the sensing board. A wired up example is shown in Figure 2.

5 PRELIMINARY EXPERIMENT

We ran a preliminary experiment to (1) verify that deforming a conductive shear cell indeed leads to changes in capacitance, and (2) determine the smallest cell size at which capacitance changes can still be detected reliably (smaller cell sizes are more desirable since they allow for more degrees of freedom in configuring metamaterial objects). For the experiment, we fabricated basic cell structures of varying width *w* and length *l*, and also varied wall thickness since it impacts how easily the printed objects can be deformed. We then measured their resonant frequencies under deformation and determined the resulting capacitance.

5.1 Cell Parameters

Cell Size (Length l and Width w): We fabricated 5 cell sizes with widths and lengths at 5mm increments, i.e. 25mm, 20mm, 15mm, 10mm and 5mm (Figure 5). Cells 4mm and smaller had a high print fail rate.

Wall Thickness: We fabricated each of the cell sizes with two different wall thickness: 0.5mm and 0.8mm. We chose 0.5mm as it is the thinnest wall thickness that is reliably printed by the common 3D printing nozzle (0.4mm). We added 0.8mm wall thickness as this creates more robust metamaterial structures. Wall thicknesses do not contribute to the capacitance equation in formula (1), i.e., capacitive sensing is dominated by the surface area *A* of the electrodes and distance *d* between them [20]. However, different wall thicknesses do have a structural impact and change the cell's mechanical compression ability. Thinner cells can be compressed more, which results in a larger capacitance change between the original and the deformed state. This is particularly important for small cells that have a small capacitance range due to their small electrodes. Larger cells that have a larger capacitance range can benefit from thicker walls to ensure robustness against repeated compression.
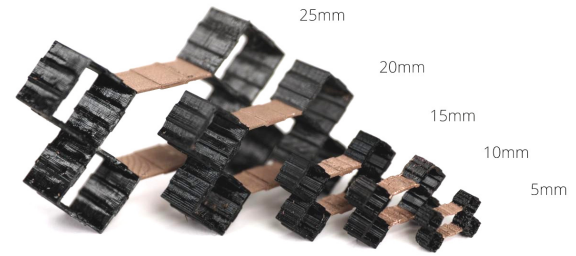

Figure 5: Cells sizes used for the evaluation: 25mm, 20mm, 15mm, 10mm, 5mm.

5.2 Experiment Setup and Procedure

Experiment Setup: For each cell size and corresponding wall thickness, we printed 5 copies for a total of 50 printed conductive shear cells (5 cell sizes × 2 thicknesses × 5 copies) and connected one copy at a time with a wire to the capacitive sensing circuit. The wire from the cell to the capacitive sensing circuit was 3cm long and isolated from human or metal disturbance by 0.5m. To be able to deform the cell without touching it, we connected a plastic strip to a digital micrometer. Adjusting the screw of the digital micrometer allowed us to precisely determine the distance between the conductive cell walls, i.e. turning the screw moved the plastic strip down, which increased the pressure on the tested cell and brought the cell walls to the specified distance.

Experiment Procedure: We measured the resonant frequencies at five different distances between the conductive cell walls. For each cell size, we divided the total distance between the two conductive cell walls by 5 to determine which distances to measure (5mm cell: measured every 1mm, 25mm cell: measured every 5mm). We measured the resonant frequency at each distance and then calculated the capacitance. Figure 6 shows an example of the capacitance when the cell is in a deformed vs. undeformed state.
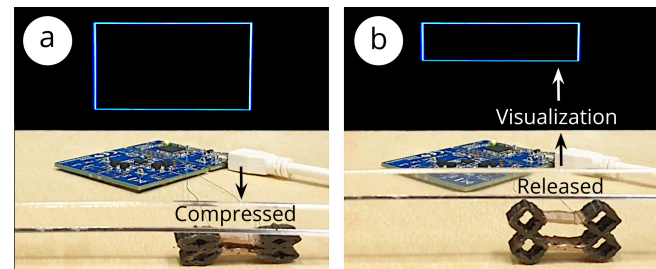

Figure 6: Visualization of capacitance in (a) compressed and (b) released states for a 5mm × 5mm × 0.5mm cell.

5.3 Experiment Results

Effect of Distance (d) on Capacitance (C): As expected, we found that the computed capacitance value *C* has an inverse relationship with the distance *d* between the opposing cell walls (Figure 7).

Effect of Cell Size (l,w) on Capacitance Range: Since capacitance is proportional to wall area (see Formula (1)), larger cells have a larger capacitance variation. This can also be seen in Figure 7 where
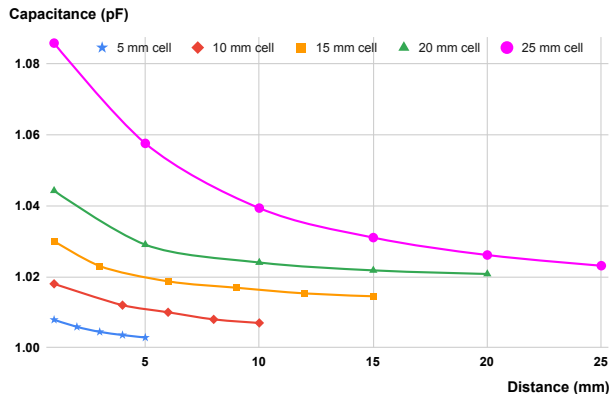
Figure 7: Measured capacitances for each cell size as the cell walls approach each other. As the distance d between cell walls decreases, capacitance C increases.

the capacitance of the largest cell (25mm) ranges from 1.022pF to 1.085pF (total range: 62.6fF) and the smallest cell (5mm) ranges from 1.005pF to 1.01pF (total range: 4.8fF). Thus, larger cell walls perform better as sensors. While our smallest 3D printable cell size still had detectable capacitance changes, the capacitance values are reaching the limit of the capacitive sensing circuit capabilities (1pF). Thus, if 3D printing resolution increases in the future and printing smaller cell sizes becomes possible, it also requires a sensing board that can sense smaller capacitance values.

Effect of Cell Size on Noise Level: We also found that larger cells are less susceptible to noise, i.e. the 25mm cell had a signal-to-noise ratio 24.4x better than that of the 5mm cell. We determine the noise level by comparing the 5 printed copies, i.e. computed the standard deviation of the overall capacitance range. For the large 25mm cells, the average capacitance range was 62.6fF with a standard deviation of 1.57E-03fF, leading to a noise level of 0.0045%, whereas for the small 5mm cells, the average capacitance range was 4.8fF with a standard deviation of 5.59E-03fF, leading to a noise level of 0.11%.

Effect of Cell Thickness on Capacitance Variation (C): As discussed previously, capacitive sensing is dominated by the surface area of the electrodes A and the distance d between electrodes [20], not the cell wall thickness. Experimentally, we confirmed that the different wall widths (0.5mm vs 0.8mm) do not have an effect on the capacitance beyond mechanical compression. At the frequencies used by the sensing chip, the wall thickness does not impact the capacitance due to the skin effect. Our signal being around 37MHz, it largely occupies less than 1μm of the surface of the copper wall (assuming a resistivity 0.012$\mu\Omega$cm).

In summary, we conclude that our sensing hardware is indeed capable of detecting the deformation of our 3D printed conductive shear cells, and that while larger cells generally perform better, our smallest cell size of 5mm still led to detectable capacitance changes.

6 3D EDITOR FOR DESIGNING METASENSE OBJECTS

To facilitate the design of MetaSense objects with integrated conductive shear cells, we implemented a voxel-style 3D editor (based on the 3D editor of metamaterial mechanisms [15]). The editor supports users in interactively placing and arranging conductive shear cells within an object's internal geometry according to the desired sensing scenario.

We illustrate our 3D editor's functionality using the example of a handheld deformable music controller that can detect user input from each of the user's fingers.

6.1 Adding Solid and Shear Cells

Adding Solid Cells: To create our music controller, we start by designing the rigid interior of the controller using solid cells (Figure 8a). We first set the cell size to 5mm using the 'cell size' input field. Next, we select the 'solid cell' type from the cell panel, select the 'add' brush, and then draw a block of solid cells for the music controller body onto the canvas.

Creating Shear Cells: Next, we create the deformable input areas by adding shear cells (Figure 8b). First, we create the deformable input area for the thumb. Since we want the thumb to shear and compress to mirror the thumbs movements, we select the 'shear cell' type from the cell panel and then draw the corresponding cells. We also want to add a metamaterial padding where the palm is touching the controller to support a firm grip. Since the palm padding should only compress and not shear, we select the 'rotated shear cell' type, which resembles a diamond shape, to draw those cells.

Adding Custom Cells: Next, we want to add the cells for the index, middle, and ring finger (Figure 8b). Since they all use the same cell design, we first create a 'custom cell' template, which is comprised of the group of cells for one finger, and save it to the custom cell menu. After this, we select our custom cell and draw each finger's input area with a single click. Similar to the palm padding, the index, middle, and ring finger input areas are designed to compress but not shear.

6.2 Specifying Object Interaction

Next, users can specify the intended object interaction by applying a force vector and simulating the deformation. This allows users to identify which parts of the cell structure deform most (i.e., have the largest capacitance variation), and are therefore the best candidate locations for placing conductive shear cells. In our music controller example, we want to specify how each finger deforms its finger padding to see where the conductive cells should be placed inside the padding.

Defining Anchor Points: We start by specifying where the finger padding of each finger is affixed on the music controller by selecting the 'anchor' tool and then placing anchor points in the corresponding location. Figure 9a shows this at the example of the finger padding for the index finger, i.e. we select the bottom left and right corners of the deformable finger padding and define them as red anchor points.

Specifying the Force Vector: Next, we specify the force that is applied to each finger padding when the user deforms it with their finger (Figure 9). To do this, we use the 'force' tool and attach a force vector to a vertex of the finger padding cell group. Next, we indicate the direction in which the force is applied. Dragging the force vector to increase its length increases the applied force. Figure 9b shows
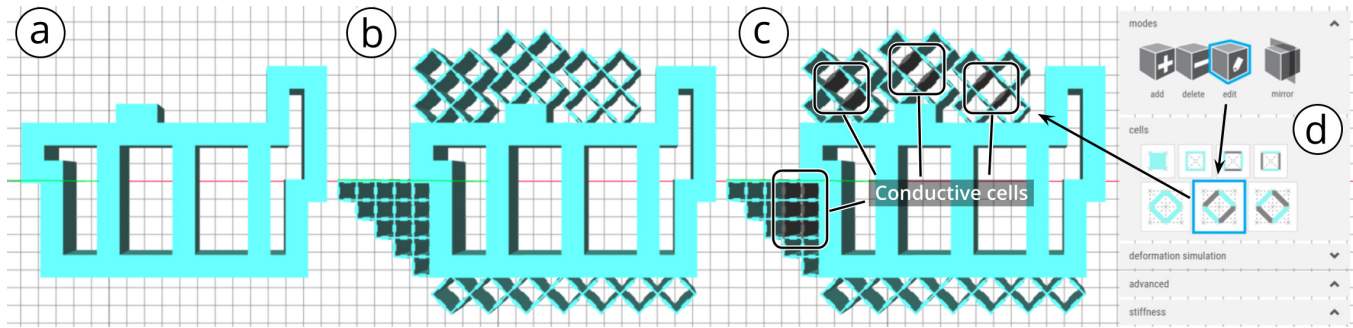
Figure 8: Creating a model in the MetaSense 3D editor: (a,b): non-conductive, structural cells; (c,d) converting structural cells to conductive cells using the edit tool.

this at the example of applying a force simulating the index finger pressing down on the deformable input area.
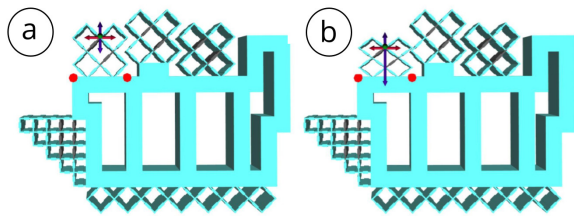
Figure 9: Specifying object interaction on our music controller. The red dots specify the locations where the finger pad is affixed. (a) Before applying the force vector, (b) after applying the force vector.

Replaying the Interaction: Our editor also supports replay. By clicking 'start', users can record the force vector manipulations with the object, and end the recording by pressing 'stop'. The provided slider can be used to replay the recorded interaction to visually confirm which cells deform most.

6.3 Placing Conductive Shear Cells

To incorporate sensing functionality into their Metasense object, users next convert cells in the best sensing locations into conductive shear cells. In our example, we want to convert one cell in each finger's deformable input area to a conductive cell to be able to sense input from the respective finger.

Manually Adding Conductive Shear Cells: Based on the force simulating, we can see that for the index, middle, and ring finger, the center cell in the cell group deforms most. We thus convert this cell in each finger's cell group into a conductive cell. To do this, we open the 'cells' panel (Figure 8d), choose the 'conductive shear cell', select the 'edit' tool, and then click on the center cell to convert it. For the thumb, we convert the second row of cells into conductive cells because our simulation shows they deform most.

Auto-placing Conductive Shear Cells: Alternatively, our editor can automatically place conductive shear cells in the locations that experience the highest deformation during interaction. Users start by specifying the number of cells they would like to convert into

conductive shear cells, which depends on the sensing application. Next, they click the 'generate' button, which automatically places the cells in the best location. In cases where the auto-placement results in conductive cells being placed too close to where a person might hold the object, users can manually change the cells using the 'edit' brush.

6.4 Exporting the Design

After completing the design, users can click 'export' to generate two .stl files, one for the conductive and one for the non-conductive filament. Users then import these files into the slicing software for the 3D printer (e.g., FlashPrint, CURA), merge them, and fabricate them using dual-material printing. The printed music controller from our walkthrough is shown in Figure 10.
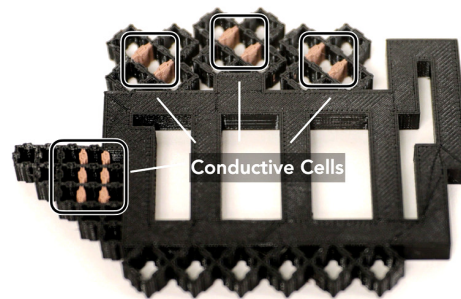
Figure 10: Printed music controller with deformable input areas for each finger.

7 AUTO-PLACEMENT ALGORITHM

To auto-place conductive shear cells, we adapt the simulation function in the metamaterial mechanisms editor [15], which computes the deformation of an object's geometry when a force is applied. This relies on a finite element solver, Karamba, a plug-in for Grasshopper (included in Rhino 6).

7.1 Placement of Conductive Shear Cells

To determine which shear cells should be converted into conductive cells, we compute the change in distance d and change in

overlapping area A for each pair of opposing walls when the cell is deformed from its original state to its deformed state. We then input the change in distance d and overlapping area A into Formula (1) to obtain the theoretical capacitance change for each pair of opposing walls. The larger the capacitance change, the more effective a cell is as a sensor. Since a single cell has two pairs of opposing walls (left and right, front and back), but only one pair of opposing walls can be used for sensing, we use the walls with the largest capacitance change to represent the quality of the cell as a sensor.

7.2 Challenges in Calculating the Change in Distance d and Area A

To determine the extent to which the capacitance changes, we need to compute the distance d and the overlapping area A before and after deformation. To accomplish this, we initially considered treating each opposing cell wall as a plane and then computing the distance d and overlapping area A between the two planes. However, we found that several factors required us to adjust our approach:

Parallel vs. Nonparallel Cell Walls: In an undeformed state, opposing walls are parallel and thus determining the distance d and overlapping area A between the two planes is straightforward. However, after deformation, walls may no longer be parallel, complicating the computation.

Coplanar and Non-Coplanar Cell Wall Vertices: Before deformation, the four vertices of a cell wall are co-planar and thus it is straightforward to determine the plane they lie in. However, after deformation this may no longer be the case and identifying a representative plane is more difficult.

Because of this, rather than basing our computation of d and A on opposing planes, we base our estimation on the individual four vertices that make up each cell wall. We then approximate the values for distance d and overlapping area A based on the relationship of the vertices to each other as described in the next section.

7.3 Estimating Changes in Distance d

For the distance d estimation, we compute the sum of Euclidean distances between the four vertex pairs at the corners of the two opposing cell walls. For example, as shown in Figure 11, the distance between the left and right wall (highlighted in grey) is defined by the sum of distances between the opposing vertices, with the left wall consisting of vertices A_1, A_2, A_3, and A_4, and the right wall consisting of vertices B_1, B_2, B_3, and B_4. The distance d can then be calculated using Formula (3):

$$Dist(left, right) = \sum_{i=1}^{4} eu\_dist\,(A_i, B_i) \quad (3)$$

After computing the distance between opposing walls before and after deformation using Formula (3), the change in distance can be calculated by subtracting the distance d' of the deformed state from the original distance d of the undeformed state as shown in Formula (4):

$$Dist\_Change = |\sum_{i=1}^{4} eu\_dist\,(A_i, B_i) - \sum_{i=1}^{4} eu\_dist\,(A'_i, B'_i)| \quad (4)$$
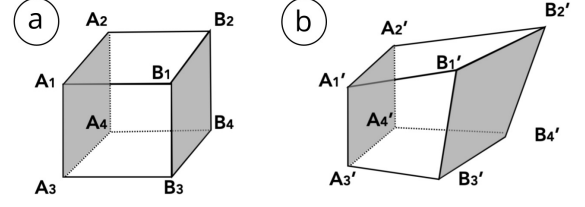

Figure 11: Computing distance d based on the vertices of the opposing walls. (a): original state; (b): deformed state.

7.4 Estimating Changes in Area A

Similar to the estimation of the change in distance, we use four vertex pairs at the corners of two opposing walls to estimate the change in the overlapping area A before and after deformation.

Computing Best-Fit Planes for Deformed Cell Walls: As discussed, the four vertices within a wall may not be coplanar after deformation. Thus, we first derive best-fit planes using the four vertices at the corners of a wall by minimizing the sum of the quadratic distances (perpendicular to the plane) between the planes and the vertices. This can be solved by calculating the singular value decomposition of the vertices' 3D coordinates [1]. We then project the original vertices (e.g., A1) onto the fitted planes (Figure 12a) and obtain the projected vertices' coordinates (e.g., A1p).
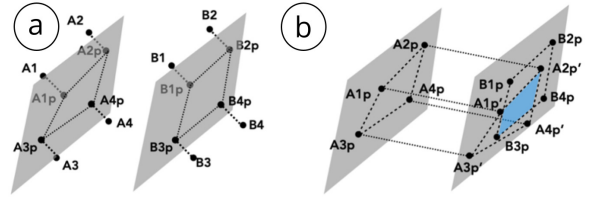

Figure 12: Overlapping area estimation: (a) project vertices onto best-fit planes; (b) find overlapping area (blue).

Projecting Vertices on a Single Plane: Since opposing planes may no longer be parallel after deformation, we project the vertices from one fitted plane (e.g., A1p) to the opposite one (e.g., A1p'). For each cell, the outcome of this projection are two co-planar quadrilaterals (Figure 12b).

Computing the Overlapping Area A: We then use the Sutherland-Hodgman polygon clipping algorithm [36] to identify the polygon created by projecting the two opposing walls onto a single plane (Figure 12b). We then compute area of the polygon using the shoelace algorithm [5].

7.5 Determining Largest Capacitance Change based on d and A

Using the approximated values for the distance d change and overlapping area A change, we can use Formula (1) to determine which pair of shear cell walls has the largest capacitance variation. For this, we divide the estimated change in area by the change in distance for each pair of opposing cell walls. We then use the shear

cell with the largest capacitance variation as the conductive shear cell, i.e. sensor.

8 APPLICATIONS

To showcase MetaSense and its integrated sensing capabilities, we created four demo objects with different usage scenarios. Each application demonstrates interactions enabled by integrating sensing into the metamaterial structure, including sensing magnitude and direction of applied force, sensing of acceleration, and input capabilities for deformable user interfaces.

8.1 Deformable User Interfaces

In the field of HCI, deformable user interfaces have gained traction and resulted in a number of different interactive devices [4]. MetaSense supports designers in quickly prototyping such deformable user interfaces by affording them with the ability to test and tweak the ergonomics and performance of their design with minimal manual labor. As an example, we developed a music controller, i.e. an input device for a digital synthesizer. As described in the walkthrough, each finger can provide input via a deformable finger padding that contains a conductive shear cell. The sensed finger input is then communicated to a Max MSP patch to influence the parameters for musical synthesis.
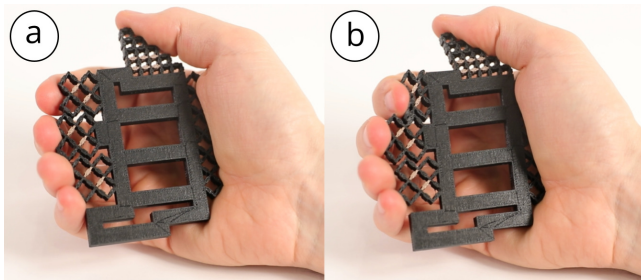
Figure 13: Ergonomic music controller: (a) undeformed state, (b) index finger applying pressure.

8.2 Sensing Magnitude and Direction of Applied Force

We designed a metamaterial joystick to demonstrate the effectiveness of MetaSense in creating monolithic tangible interfaces that can sense magnitude and direction of applied force. Figure 14 shows how we use the metamaterial joystick to play a game of PAC-MAN.

To create the joystick, we embedded four conductive cells, one in each direction of the joystick (up, down, left, right). For each conductive cell, one cell wall is contained in the moving joystick, the opposing cell wall is contained in the rigid frame. Thus, as the joystick moves inside the frame, the distance and area between the opposing cell walls changes and the direction and magnitude of applied force can be sensed. We created a custom linear regression model to convert the capacitance values from the four sensing cells into signals for the game.

The basic design of the joystick can serve as a module for designers to build on. For instance, designers can prototype various
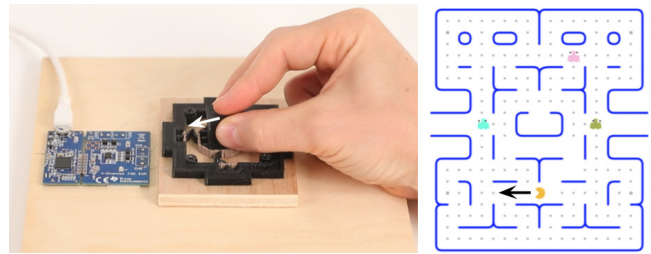
Figure 14: Monolithic metamaterial joystick that can sense magnitude and direction of applied force to control a PAC-MAN game.

tangible affordances by creating a taller grip for the joystick or making various handle shapes, including unique controllers for people with limited grip strength in particular directions.

8.3 Sensing Acceleration

Another benefit of MetaSense is its ability to integrate sensors into the structure of single part compliant mechanisms. In Figure 15, we demonstrate this capability at the example of an accelerometer. When acceleration is applied, the center 'hammer' swings towards (or away from) the conductive cell on the bordering wall. The change in capacitance can then be used to calculate the acceleration. To build the conductive part of the 'hammer', we created a custom diagonal cell in the 3D editor using the 'advanced' panel. This acts as an electrical ground shared between the two outer electrodes. As in the previous joystick example, we created a differential model to obtain measures robust to noise.

The accelerometer is one example of a capacitive sensor fabricated in a single part. Other types of capacitive sensors, such as humidity and temperature sensors, can also be fabricated in a similar manner.
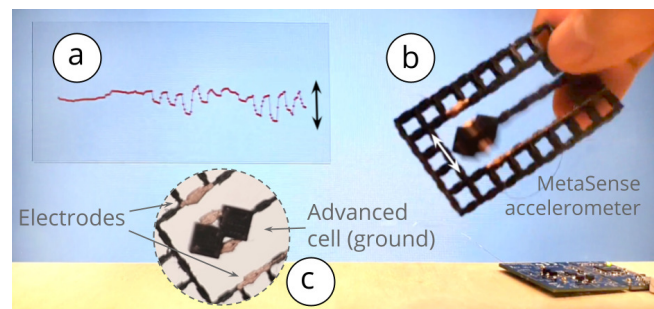
Figure 15: Accelerometer: (a) visualization of the signal, (b) fabricated accelerometer, which uses (c) two electrodes that share one ground connection.

8.4 Sensing Binary State

Mechanical engineering research has shown the benefits of compliant mechanisms that achieve force and motion transmission through elastic body deformation. The integration of conductive

shear cells into such structures adds the benefit of various built-in sensing capabilities.

We demonstrate this with a bi-stable switch that detects state transitions. This switch design is inspired by mechanisms used for latching or deploying space systems such as deployable solar arrays [44]. We embedded eight conductive shear cells into the sides of the switch. When the switch is actuated, pressure is exerted on the sides of the switch and the conductive shear cells get compressed (Figure 16). A simple threshold on the computed capacitance can be used to determine which state the switch is in. While we used eight conductive shear cells to improve robustness, a single shear cell on one side of the switch is sufficient to detect the interaction.
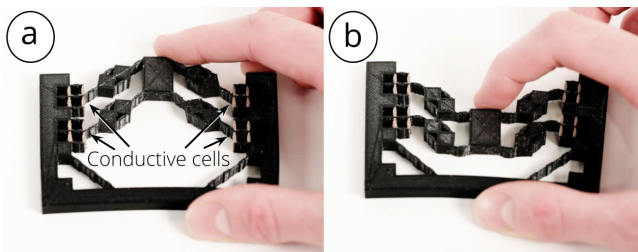
Figure 16: A bi-stable switch based on a compliant mechanism with integrated conductive shear cells for sensing when the switch is flipped: (a) off state, (b) on state.

9 DISCUSSION AND LIMITATIONS

We discuss insights gained from our work, propose future research, and acknowledge the limitations of our approach.

Auto-placing Algorithm: The accuracy of our auto-placement algorithm depends on the accuracy of the Karamba physics simulation, which we did not evaluate. As structural simulation tools improve, our auto-placement algorithm will become more accurate in predicting the most optimal locations for conductive cells. In addition, our algorithm currently does not consider the capacitive effect from neighboring conductive cells or from a user's hand during interaction when estimating optimal locations for conductive shear cells. As mentioned in Section 6, after conductive shear cells have been automatically placed, users can still override individual conductive cell locations to meet specific requirements and considerations.

Routing Traces: Currently, we use bare nickel chromium wire to connect conductive cell walls to our sensing hardware to retrieve the resonant frequency values. Adding the wires can become a tedious post-processing step if there are many conductive cells within the interior structure. One potential solution is to automatically generate conductive routes from all conductive cells, which form wires when 3D printed with conductive filament. Another possible solution is to have a conductive routing layer with various routing traces propagate through the object geometry, similar to a Printed Circuit Board (PCB). However, these ideas require further investigation to determine feasible trace widths and lengths.

Proximity of User's Hand: As a hand approaches a capacitive cell, the capacitive noise increases. For the 5mm cell, the noise is 1% when the hand is 40mm away and 10% when the hand is within 10mm. The affected region is larger for bigger cells, i.e. for the

25mm cell, 1% noise occurs 75mm away, and 10% within 15 mm. The effect of touching can be mitigated through calibration, as we did in the music controller application. As discussed, our editor also allows users to manually move the conductive cells if the auto-placement results in cells too close to where the interactions occur. Our metamaterial devices performed reliably when fingers are as close as 5mm away from the conductive cells.

Material and Durability: We did not flex the materials beyond their limits. Our 3D printed objects did not show material fatigue even after repeated use for our tests. However, depending on the brand, the elasticity of the conductive filament and non-conductive filament may not be the same, and the intersections between these two materials may be more fragile and break apart after repeated use. We plan to add a feature into the Metasense editor to allow users to increase the density of material along intersections between different materials to avoid delamination.

10 CONCLUSION

In this paper, we presented an approach to integrate sensing capabilities into 3D printable metamaterial structures by converting selected metamaterial shear cells into conductive cells. By sensing the change in capacitance when opposing cell walls are deformed, we were able to determine user interaction with the metamaterial structure. We demonstrated the functionality of our interactive 3D editor that allows designers to prototype the internal structure of metamaterial objects with integrated sensing capabilities, and discussed our fabrication pipeline and sensing hardware. We also conducted an experiment to validate the feasibility of our approach, and presented a series of applications showcasing interactions enabled by our technique. Our work opens up new possibilities in creating interactive printed objects and compliant mechanisms by embedding sensing into the fabrication process. For future work, we plan to extend our fabrication pipeline to also leverage other fabrication tools and materials (e.g., laser-cut metamaterial structures made of thin sheet material, such as paper and plastics [34]).

ACKNOWLEDGMENTS

REFERENCES

[1] K. S. Arun, T. S. Huang, and S. D. Blostein. 1987. Least-Squares Fitting of Two 3-D Point Sets. *IEEE Transactions on Pattern Analysis and Machine Intelligence* PAMI-9, 5 (Sept. 1987), 698–700. https://doi.org/10.1109/tpami.1987.4767965

[2] Autodesk. 2021. *Connected software for additive manufacturing, design and simulation.* Retrieved Jun 25 from http://autodesk.com/products/netfabb

[3] Patrick Baudisch and Stefanie Mueller. 2017. Personal Fabrication. *Foundations and Trends® in Human–Computer Interaction* 10, 3–4 (2017), 165–293. https://doi.org/10.1561/1100000055

[4] Alberto Boem and Giovanni Maria Troiano. 2019. Non-Rigid HCI: A Review of Deformable Interfaces and Input. In *Proceedings of the 2019 on Designing Interactive Systems Conference* (San Diego, CA, USA) *(DIS '19)*. Association for Computing Machinery, New York, NY, USA, 885–906. https://doi.org/10.1145/3322276.3322347

[5] Bart Braden. 1986. The Surveyor's Area Formula. *The College Mathematics Journal* 17, 4 (Sept. 1986), 326–337. https://doi.org/10.1080/07468342.1986.11972974

[6] Jesse Burstyn, Nicholas Fellion, Paul Strohmeier, and Roel Vertegaal. 2015. Print-Put: Resistive and Capacitive Input Widgets for Interactive 3D Prints. In *Human-Computer Interaction – INTERACT 2015*. Springer International Publishing, 332–339. https://doi.org/10.1007/978-3-319-22701-6_25

[7] Troy A. Chase and Ren C. Luo. 1995. A Flexible Capacitive Normal / Shear Tactile Force Sensor. In *ESSDERC '95: Proceedings of the 25th European Solid State Device Research Conference*. 351–355.

[8] Oliver Glauser, Daniele Panozzo, Otmar Hilliges, and Olga Sorkine-Hornung. 2019. Deformation Capture via Soft and Stretchable Sensor Arrays. *ACM Transactions on Graphics* 38, 2 (April 2019), 1–16. https://doi.org/10.1145/3311972

[9] Babak Haghpanah, Hamid Ebrahimi, Davood Mousanezhad, Jonathan Hopkins, and Ashkan Vaziri. 2015. Programmable Elastic Metamaterials. *Advanced Engineering Materials* 18, 4 (Oct. 2015), 643–649. https://doi.org/10.1002/adem.201500295

[10] Charles El Helou, Philip R. Buskohl, Christopher E. Tabor, and Ryan L. Harne. 2021. Digital logic gates in soft, conductive mechanical metamaterials. *Nature Communications* 12, 1 (March 2021). https://doi.org/10.1038/s41467-021-21920-y

[11] Texas Instruments. 2021. *Capacitive Proximity Sensing Using FDC2x1y*. Retrieved Jun 25 from https://www.ti.com/lit/an/slya048b/slya048b.pdf

[12] Texas Instruments. 2021. *Common Inductive & Capacitive Sensing Applications*. Retrieved Jun 25 from http://ti.com/lit/an/slya048a/slya048a.pdf

[13] Alexandra Ion, Johannes Frohnhofen, Ludwig Wall, Robert Kovacs, Mirela Alistar, Jack Lindsay, Pedro Lopes, Hsiang-Ting Chen, and Patrick Baudisch. 2016. Metamaterial Mechanisms. In *Proceedings of the 29th Annual Symposium on User Interface Software and Technology*. ACM. https://doi.org/10.1145/2984511.2984540

[14] Alexandra Ion, Ludwig Wall, Robert Kovacs, and Patrick Baudisch. 2017. Digital Mechanical Metamaterials. In *Proceedings of the 2017 CHI Conference on Human Factors in Computing Systems*. ACM. https://doi.org/10.1145/3025453.3025624

[15] Vikram Iyer, Justin Chan, and Shyamnath Gollakota. 2017. 3D printing wireless connected objects. *ACM Transactions on Graphics* 36, 6 (Nov. 2017), 1–13. https://doi.org/10.1145/3130800.3130822

[16] Lin Lu, Andrei Sharf, Haisen Zhao, Yuan Wei, Qingnan Fan, Xuelin Chen, Yann Savoye, Changhe Tu, Daniel Cohen-Or, and Baoquan Chen. 2014. Build-to-last. *ACM Transactions on Graphics* 33, 4 (July 2014), 1–10. https://doi.org/10.1145/2601097.2601168

[17] Karola Marky, Martin Schmitz, Verena Zimmermann, Martin Herbers, Kai Kunze, and Max Mühlhäuser. 2020. 3D-Auth: Two-Factor Authentication with Personalized 3D-Printed Items. In *Proceedings of the 2020 CHI Conference on Human Factors in Computing Systems*. ACM. https://doi.org/10.1145/3313831.3376189

[18] Materialise. 2021. *Premium data optimization software*. Retrieved Jun 25 from http://materialise.com/en/software/3-matic

[19] Zachary H. Nick, Christopher E. Tabor, and Ryan L. Harne. 2020. Liquid metal microchannels as digital sensors in mechanical metamaterials. *Extreme Mechanics Letters* 40 (2020), 100871. https://doi.org/10.1016/j.eml.2020.100871

[20] Stoyan Nihtianov. 2014. Measuring in the Subnanometer Range: Capacitive and Eddy Current Nanodisplacement Sensors. *IEEE Industrial Electronics Magazine* 8, 1 (2014), 6–15. https://doi.org/10.1109/MIE.2013.2285240

[21] Simon Olberding, Sergio Soto Ortega, Klaus Hildebrandt, and Jürgen Steimle. 2015. Foldio. In *Proceedings of the 28th Annual ACM Symposium on User Interface Software & Technology*. ACM. https://doi.org/10.1145/2807442.2807494

[22] Johannes T.B. Overvelde, Twan A. de Jong, Yanina Shevchenko, Sergio A. Becerra, George M. Whitesides, James C. Weaver, Chuck Hoberman, and Katia Bertoldi. 2016. A three-dimensional actuated origami-inspired transformable metamaterial with multiple degrees of freedom. *Nature Communications* 7, 1 (March 2016). https://doi.org/10.1038/ncomms10929

[23] Johannes T. B. Overvelde, James C. Weaver, Chuck Hoberman, and Katia Bertoldi. 2017. Rational design of reconfigurable prismatic architected materials. *Nature* 541, 7637 (Jan. 2017), 347–352. https://doi.org/10.1038/nature20824

[24] Jayson Paulose, Anne S. Meeussen, and Vincenzo Vitelli. 2015. Selective buckling via states of self-stress in topological metamaterials. *Proceedings of the National Academy of Sciences* 112, 25 (June 2015), 7639–7644. https://doi.org/10.1073/pnas.1502939112

[25] Romain Prévost, Emily Whiting, Sylvain Lefebvre, and Olga Sorkine-Hornung. 2013. Make it stand. *ACM Transactions on Graphics* 32, 4 (July 2013), 1–10. https://doi.org/10.1145/2461912.2461957

[26] Mirza Saquib us Sarwar. 2019. *Soft capacitive sensors for proximity, touch, pressure and shear measurements*. Ph.D. Dissertation. University of British Columbia. https://doi.org/10.14288/1.0378695

[27] Valkyrie Savage, Ryan Schmidt, Tovi Grossman, George Fitzmaurice, and Björn Hartmann. 2014. A series of tubes. In *Proceedings of the 27th annual ACM symposium on User interface software and technology*. ACM. https://doi.org/10.1145/2642918.2647374

[28] Valkyrie Savage, Xiaohan Zhang, and Björn Hartmann. 2012. Midas. In *Proceedings of the 25th annual ACM symposium on User interface software and technology - UIST '12*. ACM Press. https://doi.org/10.1145/2380116.2380189

[29] Martin Schmitz, Mohammadreza Khalilbeigi, Matthias Balwierz, Roman Lissermann, Max Mühlhäuser, and Jürgen Steimle. 2015. Capricate. In *Proceedings of the 28th Annual ACM Symposium on User Interface Software & Technology*. ACM. https://doi.org/10.1145/2807442.2807503

[30] Martin Schmitz, Jürgen Steimle, Jochen Huber, Niloofar Dezfuli, and Max Mühlhäuser. 2017. Flexibles. In *Proceedings of the 2017 CHI Conference on Human Factors in Computing Systems*. ACM. https://doi.org/10.1145/3025453.3025663

[31] Martin Schmitz, Martin Stitz, Florian Müller, Markus Funk, and Max Mühlhäuser. 2019. ./trilaterate. In *Proceedings of the 2019 CHI Conference on Human Factors in Computing Systems*. ACM. https://doi.org/10.1145/3290605.3300684

[32] Christian Schumacher, Bernd Bickel, Jan Rys, Steve Marschner, Chiara Daraio, and Markus Gross. 2015. Microstructures to control elasticity in 3D printing. *ACM Transactions on Graphics* 34, 4 (July 2015), 1–13. https://doi.org/10.1145/2766926

[33] Sicong Shan, Sung H. Kang, Jordan R. Raney, Pai Wang, Lichen Fang, Francisco Candido, Jennifer A. Lewis, and Katia Bertoldi. 2015. Multistable Architected Materials for Trapping Elastic Strain Energy. *Advanced Materials* 27, 29 (June 2015), 4296–4301. https://doi.org/10.1002/adma.201501708

[34] Madlaina Signer, Alexandra Ion, and Olga Sorkine-Hornung. 2021. Developable Metamaterials: Mass-fabricable Metamaterials by Laser-Cutting Elastic Structures. In *Proceedings of the 2021 CHI Conference on Human Factors in Computing Systems*. 1–13.

[35] Ronit Slyper, Ivan Poupyrev, and Jessica Hodgins. 2010. Sensing through structure. In *Proceedings of the fifth international conference on Tangible, embedded, and embodied interaction*. ACM. https://doi.org/10.1145/1935701.1935744

[36] Ivan E. Sutherland and Gary W. Hodgman. 1974. Reentrant polygon clipping. *Commun. ACM* 17, 1 (Jan. 1974), 32–42. https://doi.org/10.1145/360767.360802

[37] Nobuyuki Umetani and Ryan Schmidt. 2017. SurfCuit: Surface-Mounted Circuits on 3D Prints. *IEEE Computer Graphics and Applications* 37, 3 (May 2017), 52–60. https://doi.org/10.1109/mcg.2017.40

[38] Tatyana Vasilevitsky and Amit Zoran. 2016. Steel-Sense. In *Proceedings of the 2016 CHI Conference on Human Factors in Computing Systems*. ACM. https://doi.org/10.1145/2858036.2858309

[39] Kiril Vidimce, Alexandre Kaspar, Ye Wang, and Wojciech Matusik. 2016. Foundry. In *Proceedings of the 29th Annual Symposium on User Interface Software and Technology*. ACM. https://doi.org/10.1145/2984511.2984516

[40] Kiril Vidimče, Szu-Po Wang, Jonathan Ragan-Kelley, and Wojciech Matusik. 2013. OpenFab. *ACM Transactions on Graphics* 32, 4 (July 2013), 1–12. https://doi.org/10.1145/2461912.2461993

[41] Michael Wessely, Ticha Sethapakdi, Carlos Castillo, Jackson C. Snowden, Ollie Hanton, Isabel P. S. Qamar, Mike Fraser, Anne Roudaut, and Stefanie Mueller. 2020. *Sprayable User Interfaces: Prototyping Large-Scale Interactive Surfaces with Sensors and Displays*. Association for Computing Machinery, New York, NY, USA, 1–12. https://doi.org/10.1145/3313831.3376249

[42] Yang Zhang, Gierad Laput, and Chris Harrison. 2017. Electrick. In *Proceedings of the 2017 CHI Conference on Human Factors in Computing Systems*. ACM. https://doi.org/10.1145/3025453.3025842

[43] Junyi Zhu, Lotta-Gili Blumberg, Yunyi Zhu, Martin Nisser, Ethan Levi Carlson, Xin Wen, Kevin Shum, Jessica Ayeley Quaye, and Stefanie Mueller. 2020. *CurveBoards: Integrating Breadboards into Physical Objects to Prototype Function in the Context of Form*. Association for Computing Machinery, New York, NY, USA, 1–13. https://doi.org/10.1145/3313831.3376617

[44] Shannon A. Zirbel, Kyler A. Tolman, Brian P. Trease, and Larry L. Howell. 2016. Bistable Mechanisms for Space Applications. *PLOS ONE* 11, 12 (Dec. 2016), e0168218. https://doi.org/10.1371/journal.pone.0168218